

Vortex-lattice formation in a spin-orbit coupled rotating spin-1 condensate

S. K. Adhikari*

Instituto de Física Teórica, Universidade Estadual Paulista - UNESP, 01.140-070 São Paulo, São Paulo, Brazil

(Dated: October 9, 2020)

We study the vortex-lattice formation in a rotating Rashba spin-orbit (SO) coupled quasi-two-dimensional (quasi-2D) hyper-fine spin-1 spinor Bose-Einstein condensate (BEC) in the $x-y$ plane using a numerical solution of the underlying mean-field Gross-Pitaevskii equation. In this case, the non-rotating Rashba SO-coupled spinor BEC can have topological excitation in the form of vortices of different angular momenta in the three components, e.g. the $(0, +1, +2)$ - and $(-1, 0, +1)$ -type states in ferromagnetic and anti-ferromagnetic spinor BEC: the numbers in the parenthesis denote the intrinsic angular momentum of the vortex states of the three components with the negative sign denoting an anti-vortex. The presence of these states with intrinsic vorticity breaks the symmetry between rotation with vorticity along the z and $-z$ axes and thus generates a rich variety of vortex-lattice and anti-vortex-lattice states in a rotating quasi-2D spin-1 spinor ferromagnetic and anti-ferromagnetic BEC, not possible in a scalar BEC. For weak SO coupling, we find two types of symmetries of these states – hexagonal and “square”. The hexagonal (square) symmetry state has vortices arranged in closed concentric orbits with a maximum of 6, 12, 18... (8, 12, 16...) vortices in successive orbits. Of these two symmetries, the square vortex-lattice state is found to have the smaller energy.

I. INTRODUCTION

After the observation of a trapped Bose-Einstein condensate (BEC) in ^{87}Rb and ^{23}Na alkali metal atoms at ultra-low temperature in a laboratory [1], rotating trapped condensates hosting quantized vortices [2] and large vortex lattices [3] were created, for small and large angular frequencies of rotation, respectively, under controlled conditions and studied experimentally. As suggested by Onsager [4], Feynman [5] and Abrikosov [6] these vortices have quantized circulation as in liquid He II [7]

$$\frac{\tilde{m}}{2\pi\hbar} \oint_{\mathcal{C}} \mathbf{v} \cdot d\mathbf{r} = \pm l, \quad (1)$$

where $\mathbf{v}(\mathbf{r}, t)$ is the super-fluid velocity field at a space point \mathbf{r} and time t , \mathcal{C} is a generic closed path, l is the quantized angular momentum of an atom in units of \hbar in the rotating BEC and \tilde{m} is the mass of an atom. For notational simplicity, the circulation (1) is scaled by a factor of $2\pi\hbar/\tilde{m}$, so that its absolute value is equal to angular momentum l : a positive (negative) circulation corresponds to a vortex (anti-vortex). If $l \neq 0$, there are topological defects inside the closed path \mathcal{C} , which manifests in the form of a quantized vortex line [7]. Quantized vortices of unit angular momentum were first observed in a uniform super-fluid He II in a rotating bucket [8]. Vorticity is the curl of the velocity field $\nabla_{\mathbf{r}} \times \mathbf{v}(\mathbf{r}, t)$ and determines the direction of the angular momentum vector. London gave a qualitative explanation of quantization of circulation in He II [9]. In addition, if we assume that the dynamics of the super-fluid is governed by a

complex scalar field $\phi(\mathbf{r}, t) \equiv |\psi(\mathbf{r}, t)| \exp[i\delta(\mathbf{r}, t)]$ with $\mathbf{v}(\mathbf{r}, t) = \nabla_{\mathbf{r}}\delta(\mathbf{r}, t)$, then $\psi(\mathbf{r}, t)$ is known to satisfy the mean-field Gross-Pitaevskii (GP) equation [7] which has been used successfully to study the formation of vortex and vortex lattice [10] in a BEC.

A spinor BEC of ^{23}Na atoms [11] with hyper-fine spin $F = 1$ has also been observed and, more recently, it has been possible to introduce an artificial synthetic SO coupling by Raman lasers that coherently couple the spin-component states in a spinor BEC [12]. Two common SO couplings are due to Rashba [13] and Dresselhaus [14]. An equal mixture of these SO couplings has been realized in pseudo spin-1/2 ^{87}Rb [15] and ^{23}Na [16] BECs containing only two spin components $F_z = 0, -1$ of total spin $F = 1$. Later, an equal mixture of Rashba and Dresselhaus SO couplings has also been created in a spin-1 ferromagnetic ^{87}Rb BEC, containing all three spin components $F_z = \pm 1, 0$ [17].

Spinor BECs can show a rich variety of topological excitation [18–21] not possible in a scalar BEC. The predicted Mermin-Ho [22] and Anderson-Toulouse [23] vortices in ^3He with a non-singular angular momentum structure, although not observed in ^3He , might appear in a spinor BEC. It was later demonstrated [20] that, in a trapped slowly rotating ferromagnetic spinor BEC, the Mermin-Ho and Anderson-Toulouse vortices are thermodynamically stable. Such stable vortices appear in a ferromagnetic spinor BEC in the form of a state of type $(0, +1, +2)$ [19, 20], where the numbers in the parenthesis denote the circulation (angular momentum) of vortices in components $F_z = +1, 0, -1$, respectively. For certain values of magnetization, $(+1, +1, +1)$ and $(+1, 0, -1)$ -type states are also demonstrated to appear [20] in a ferromagnetic spinor BEC. The $(+1, 0, -1)$ -type state hosts a vortex (anti-vortex of negative vorticity) in the component $F_z = +1$ ($F_z = -1$), whereas the component $F_z = 0$ remains vortex free. However, such states in an

*s.k.adhikari@unesp.br,
<https://professores.ift.unesp.br/sk.adhikari>

anti-ferromagnetic BEC were not found to be stable [20]. The analogue of these states in a pseudo spin-1/2 system is the $(0, +1)$ -type half-quantum state [24–26].

In bosonic spin systems, SO-coupling leads to a variety of novel phenomena that are not possible in spinor BECs without SO coupling [27], for example [28], the stripe phase [29, 30], the Rashba pairing bound states (Rashbons) [31], spin Hall effect [32], spintronics [33], as well as the super-fluidity and Mott-insulator phases of SO-coupled quantum gases in optical lattice [34]. A three-component SO-coupled spin-1 BEC is known to exhibit a rich variety of physical phenomena not possible in a two-component pseudo spin-1/2 BEC [18, 29, 35]. A spin-1 spinor BEC is controlled by two interaction strengths, e.g., $c_0 \propto (a_0 + 2a_2)/3$ and $c_2 \propto (a_2 - a_0)/3$, with a_0 and a_2 the scattering lengths in total spin 0 and 2 channels, respectively, and appears in two distinct phases: ferromagnetic ($c_2 < 0$) and anti-ferromagnetic or polar ($c_2 > 0$).

In view of this, we investigate in this paper the formation of vortex lattice in a rapidly rotating Rashba SO-coupled ferromagnetic and anti-ferromagnetic trapped spin-1 spinor BEC, to see the effect of the above topological excitation in the generated vortex lattice, if any. Previously, the formation of vortex and vortex lattice in a Rashba SO-coupled trapped pseudo spin-1/2 spinor BEC was studied numerically [24, 25] and analytically [26]. Different ways of realizing a rotating SO-coupled spinor BEC have been suggested [36]. We find that for a weakly Rashba SO-coupled quasi-two-dimensional (quasi-2D) non-rotating ferromagnetic spin-1 spinor BEC, the lowest-energy circularly-symmetric state is a $(0, +1, +2)$ -type state [37]. For a weakly Rashba SO-coupled quasi-2D non-rotating anti-ferromagnetic spinor BEC, the lowest-energy circularly-symmetric state is of the type $(-1, 0, +1)$ [37]. In a rotating quasi-2D scalar BEC in the $x - y$ plane, the generated vortex-lattice structure is the same for vorticity of rotation along z or $-z$ axis. However, the generated vortex lattice for vorticity of rotation along z or $-z$ axis will be different for a Rashba SO-coupled spin-1 spinor BEC because of the above symmetry-breaking $(0, +1, +2)$ and $(-1, 0, +1)$ -type states. When subject to rotation, both ferromagnetic and anti-ferromagnetic spinor BECs form vortex lattices with a hexagonal or an *approximate* “square” symmetry. Although, the square symmetry is often distorted, from a study of energies, distinct from a rotating scalar BEC, it was found that the lattice structure with square symmetry has the smaller energy. In case of a scalar BEC the vortex lattice with hexagonal symmetry has the smallest energy. In the case of a ferromagnetic Rashba SO-coupled spin-1 spinor BEC, for rotation with vorticity along z direction, the hexagonal or square vortex-lattice structure is built around the $(0, +1, +2)$ -type state at the center: the central site of the three components $F_z = +1, 0, -1$, respectively, host vortices of circulation $0, +1, +2$. For rotation with vorticity along $-z$ direction, an anti-vortex lattice is

generated in both ferromagnetic and anti-ferromagnetic spinor BEC around a complex anti-vortex structure at the center.

In Sec. II we present the mean-field GP equation for a rotating quasi-2D SO-coupled spin-1 spinor condensate in the rotating frame. In Sec. III we present the numerical details for the solution of the GP equation as well as the numerical results obtained from its solution for weak SO coupling using the split-time-step Crank-Nicolson discretization scheme. For rotation with angular momentum along z and $-z$ directions, the generated vortex- and anti-vortex-lattice structures with hexagonal and square symmetries were studied for ferromagnetic and anti-ferromagnetic spinor BECs. Finally, in Sec. V we present a summary of our study.

II. THE GROSS-PITAEVSKII EQUATION FOR A ROTATING SPIN-1 CONDENSATE

We will consider a Rashba SO-coupled BEC with coupling between the spin and momentum given by $\gamma(\Sigma_x p_y - \Sigma_y p_x)$ [15], where γ is the strength of SO coupling, p_x and p_y are the x and y components of the momentum operator and Σ_x and Σ_y are the irreducible representations of the x and y components of the spin matrix, respectively,

$$\Sigma_x = \frac{1}{\sqrt{2}} \begin{pmatrix} 0 & 1 & 0 \\ 1 & 0 & 1 \\ 0 & 1 & 0 \end{pmatrix}, \quad \Sigma_y = \frac{i}{\sqrt{2}} \begin{pmatrix} 0 & -1 & 0 \\ 1 & 0 & -1 \\ 0 & 1 & 0 \end{pmatrix}. \quad (2)$$

For the study of vortex-lattice formation in a rotating SO-coupled quasi-2D spin-1 spinor BEC, we consider a harmonic trap $V(\mathbf{r}) = \tilde{m}\omega^2(x^2 + y^2)/2 + \tilde{m}\omega_z^2 z^2/2$ with tighter binding in the z direction ($\omega_z \gg \omega$), where ω_z is the angular frequency of the trap in the z direction and ω that in the $x - y$ plane. The single-particle Hamiltonian of the condensate without atomic interaction and with Rashba [13] SO coupling in this quasi-2D trap, in dimensionless variables, is [15, 38]

$$H_0 = -\frac{1}{2}\nabla_{\mathbf{r}}^2 + \frac{x^2 + y^2}{2} + \frac{\omega_z^2 z^2}{2\omega^2} + \gamma(\Sigma_x p_y - \Sigma_y p_x), \quad (3)$$

where $\mathbf{r} = \{x, y, z\}$, $\nabla_{\mathbf{r}}^2 = -(p_x^2 + p_y^2 + p_z^2)$, $p_x = -i\partial_x$, $p_y = -i\partial_y$ and $p_z = -i\partial_z$ are the momentum operators along x, y and z axes, respectively, $\partial_x, \partial_y, \partial_z$ are partial space derivatives. All quantities in (3) and in the following are dimensionless; this is achieved by expressing length (x, y, z) in units of harmonic oscillator length $l_0 \equiv \sqrt{\hbar/\tilde{m}\omega}$, and energy in units of $\hbar\omega$.

The formation of a vortex lattice in a rapidly rotating spinor BEC can be conveniently studied in the rotating frame, where the generated vortex-lattice state is a stationary one, that can be obtained by the imaginary-time propagation method [7]. Such a dynamical equation in the rotating frame can be written if we note that the Hamiltonian in the rotating frame is given by $H = H_0 - \Omega_0 L_z$ [39], where H_0 is the laboratory frame

Hamiltonian, Ω_0 is the angular frequency of rotation around the z axis, and $L_z \equiv (xp_y - yp_x) = i(y\partial_x - x\partial_y)$ is the z component of the angular momentum. In a trapped condensate, for rotation around z axis, ordered vortex-lattice formation is possible for $\Omega_0 < \omega$ [7]. As Ω_0 is increased above ω , the whole super-fluid moves away from the center towards the boundary because of an excess of centrifugal force, and the super-fluidity of the condensate breaks down [7]. This was verified in our numerical calculation.

For tight harmonic binding along z direction, assuming a Gaussian density distribution in the z direction, after integrating out the z coordinate following the procedure of [40], in the mean-field approximation, a quasi-2D rotating SO-coupled spin-1 spinor BEC is described by the following set of three coupled GP equations for N atoms in dimensionless form for the hyper-fine spin components $F_z = \pm 1, 0$ [18, 41, 42]

$$i\partial_t\psi_{\pm 1}(\boldsymbol{\rho}) = [\mathcal{H} + c_2(n_{\pm 1} - n_{\mp 1} + n_0) - \Omega L_z]\psi_{\pm 1}(\boldsymbol{\rho}) + \{c_2\psi_0^2(\boldsymbol{\rho})\psi_{\mp 1}^*(\boldsymbol{\rho})\} - i\tilde{\gamma}(\partial_y\psi_0(\boldsymbol{\rho}) \pm i\partial_x\psi_0(\boldsymbol{\rho})), \quad (4)$$

$$i\partial_t\psi_0(\boldsymbol{\rho}) = [\mathcal{H} + c_2(n_{+1} + n_{-1}) - \Omega L_z]\psi_0(\boldsymbol{\rho}) + \{2c_2\psi_{+1}(\boldsymbol{\rho})\psi_{-1}(\boldsymbol{\rho})\psi_0^*(\boldsymbol{\rho})\} - i\tilde{\gamma}[-i\partial_x\{\psi_{+1}(\boldsymbol{\rho}) - \psi_{-1}(\boldsymbol{\rho})\} + \partial_y\{\psi_{+1}(\boldsymbol{\rho}) + \psi_{-1}(\boldsymbol{\rho})\}], \quad (5)$$

$$\mathcal{H} = -\frac{1}{2}\nabla_{\boldsymbol{\rho}}^2 + V(\boldsymbol{\rho}) + c_0n, \quad (6)$$

$$c_0 = \frac{2N\sqrt{2\pi\kappa}(a_0 + 2a_2)}{3}, \quad c_2 = \frac{2N\sqrt{2\pi\kappa}(a_2 - a_0)}{3}, \quad (7)$$

where $\boldsymbol{\rho} \equiv \{x, y\}$, $\nabla_{\boldsymbol{\rho}}^2 \equiv (\partial_x^2 + \partial_y^2)$, $\kappa = \omega_z/\omega$ ($\gg 1$), $\Omega = \Omega_0/\omega$ (< 1), $\tilde{\gamma} = \gamma/\sqrt{2}$, $n_j = |\psi_j|^2$, $j = \pm 1, 0$, are the component densities, in units of l_0^{-2} , of hyper-fine spin components $F_z = \pm 1, 0$ and $n(\boldsymbol{\rho}) = \sum_j n_j(\boldsymbol{\rho})$ is the total density, $V(\boldsymbol{\rho}) \equiv (x^2 + y^2)/2$ is the circularly symmetric confining trap in the $x - y$ plane, ∂_t is the partial time derivative with time in units of ω^{-1} , a_0 and a_2 are the s-wave scattering lengths, in units of l_0 , in the total spin 0 and 2 channels, respectively, and the asterisk denotes complex conjugate. The maximum allowed value of angular frequency in (4)-(5) for the formation of an ordered super-fluid vortex lattice is $|\Omega| = 1$ [7]. For notational compactness, the time dependence of the wave functions is not explicitly shown in (4) and (5). The normalization condition is $\int n(\boldsymbol{\rho}) d\boldsymbol{\rho} = 1$. Equations (4)-(5) can be derived from the energy functional [7, 18]

$$E[\psi(\Omega)] = \frac{1}{2} \int d\boldsymbol{\rho} \left\{ \sum_j |\nabla_{\boldsymbol{\rho}}\psi_j|^2 + 2Vn + c_0n^2 + c_2[n_{+1}^2 + n_{-1}^2 + 2(n_{+1}n_0 + n_{-1}n_0 - n_{+1}n_{-1}) + \psi_{-1}^*\psi_0^2\psi_{+1}^* + \psi_{-1}\psi_0^{*2}\psi_{+1}] - 2i\tilde{\gamma}[\psi_0^*\partial_y(\psi_{+1} + \psi_{-1}) + (\psi_{+1}^* + \psi_{-1}^*)\partial_y\psi_0 - i\psi_0^*\partial_x(\psi_{+1} - \psi_{-1}) + i(\psi_{+1}^* - \psi_{-1}^*)\partial_x\psi_0] - 2\Omega \sum_j \psi_j^* L_z \psi_j \right\}, \quad (8)$$

where the space dependence of different variables is not explicitly shown. The Ω dependence of the wave function is shown to recall that the energy functional is a function of the angular frequency of rotation.

III. NUMERICAL RESULTS

To solve (4) and (5) numerically, we propagate these equations in time by the split-time-step Crank-Nicolson discretization scheme [37, 43–45] using a space step of 0.1 and a time step Δ of 0.001 to obtain the stationary state by imaginary-time simulation. There are different C and FORTRAN programs for solving the GP equation [43, 44] and one should use the appropriate one. These programs have recently been adapted to simulate the vortex lattice in a rapidly rotating BEC [10] and we use these in this study.

The imaginary-time propagation is started with an appropriate initial state consistent with symmetry for quick convergence. In the ferromagnetic and anti-ferromagnetic phases, the circularly-symmetric ground states of the Rashba SO-coupled spin-1 BEC are of types $(0, +1, +2)$ and $(-1, 0, +1)$ [37], respectively, with vortices in components. In numerical simulation of vortex lattice in a rotating SO-coupled spin-1 BEC we will include these vortices in the initial state. For a final localized state without vorticity, a Gaussian initial state in each component is adequate: $\psi_j(\boldsymbol{\rho}) \sim \exp(-\rho^2/\alpha_j^2)$, where α_j is the width. However, for a $(0, +1, +2)$ -type state with vorticity, we will take the initial functions $\psi_{+1}(\boldsymbol{\rho}) \sim \exp(-\rho^2/\alpha_j^2)$, $\psi_0(\boldsymbol{\rho}) \sim (x + iy)\exp(-\rho^2/\alpha_j^2)$, $\psi_{-1}(\boldsymbol{\rho}) \sim (x + iy)^2\exp(-\rho^2/\alpha_j^2)$. Similarly, for a $(-1, 0, +1)$ -type state, we take the initial functions $\psi_{+1}(\boldsymbol{\rho}) \sim (x - iy)\exp(-\rho^2/\alpha_j^2)$, $\psi_0(\boldsymbol{\rho}) \sim \exp(-\rho^2/\alpha_j^2)$, $\psi_{-1}(\boldsymbol{\rho}) \sim (x + iy)\exp(-\rho^2/\alpha_j^2)$. With these initial states, with proper vorticity, the convergence of the imaginary-time propagation is quick.

The parameters of the GP equation c_0 and c_2 are taken from the following realistic experimental situations. For the quasi-2D ferromagnetic BEC we use the following parameters of ^{87}Rb atoms: $N = 100,000$, $a_0 = 101.8a_B$, $a_2 = 100.4a_B$, [46] $l_z \equiv l_0/\sqrt{\kappa} = 2.0157 \mu\text{m}$, where a_B is the Bohr radius. Consequently, $c_0 \equiv 2N\sqrt{2\pi}(a_0 + 2a_2)/3l_z \approx 1327$ and $c_2 \equiv 2N\sqrt{2\pi}(a_2 - a_0)/3l_z \approx -6.15$. For the quasi-2D anti-ferromagnetic BEC we use the following parameters of ^{23}Na atoms: $N = 100,000$, $a_0 = 50.00a_B$, $a_2 = 55.01a_B$, [47] $l_z = 2.9369 \mu\text{m}$. Consequently, $c_0 \approx 482$ and $c_2 \approx 15$. The ^{87}Rb and ^{23}Na atoms naturally appear in ferromagnetic ($c_2 < 0$) and anti-ferromagnetic ($c_2 > 0$) phases, respectively. Hence, to simulate a ferromagnetic (anti-ferromagnetic) BEC we use the parameters of ^{87}Rb (^{23}Na). Using a Feshbach resonance it is possible to change the sign of c_2 , thus turning, for example, a ferromagnetic ^{87}Rb BEC to an anti-ferromagnetic BEC. However, we will not consider this possibility in this paper.

A. Classification of states and symmetries

We will consider Rashba SO-coupled ferromagnetic and anti-ferromagnetic spinor BECs for weak SO coupling ($\gamma \lesssim 0.75$) and an initial circularly-symmetric solution for the quasi-2D non-rotating spinor BEC. For large values of γ , the non-rotating SO-coupled spinor BEC has stripe (and other) pattern in density [29, 30], breaking circular symmetry. The rotation of such a state should lead to a complex vortex-lattice structure and will not be considered in this paper.

The formation of vortex lattice in a scalar BEC, without intrinsic vorticity in the absence of rotation, is different from that in an SO-coupled spin-1 spinor BEC with states of type $(0, +1, +2)$ or $(-1, 0, +1)$ with intrinsic vorticity [20]. For a weakly SO-coupled spin-1 ferromagnetic spinor BEC of type $(0, +1, +2)$, rotating with the angular momentum vector parallel to the vorticity direction, a vortex lattice with hexagonal symmetry can be generated maintaining the states of circulation $+1$ and $+2$ at the center in components $j = 0$ and -1 , respectively, while the center of the $j = +1$ component is maintained vortex free. However, in this case, for rotation with the angular momentum vector anti-parallel to the vorticity direction, for small angular frequency of rotation, the state of type $(0, +1, +2)$ becomes one of type $(-2, -1, 0)$. The $(-2, -1, 0)$ -type state results upon a superposition of the $(0, +1, +2)$ -type state with a $(-2, -2, -2)$ -type state: the latter is generated by rotation. This is a two-step process. First a $(-1, 0, +1)$ -type state is formed upon the superposition of a $(-1, -1, -1)$ -type state, generated by rotation, with the $(0, +1, +2)$ -type state. Later another $(-1, -1, -1)$ -type state superposed on the $(-1, 0, +1)$ -type state yields the $(-2, -1, 0)$ -type state. With the increase of angular frequency of rotation, an anti-vortex lattice with hexagonal symmetry can be generated maintaining these central anti-vortices of circulation -2 and -1 in components $j = +1$, and 0 , respectively. The anti-vortex lattice is really a vortex lattice with opposite vorticity.

For a weakly SO-coupled spin-1 anti-ferromagnetic spinor BEC of type $(-1, 0, +1)$, rotating with the angular momentum vector parallel to the vorticity z direction, for small angular frequency of rotation, the state $(-1, 0, +1)$ transforms into the state $(0, +1, +2)$. The $(0, +1, +2)$ -type state results upon a superposition of the $(-1, 0, +1)$ -type state with a $(+1, +1, +1)$ -type state: the latter is generated by rotation. In this case, upon the increase of angular frequency of rotation, a vortex lattice with hexagonal symmetry can be generated maintaining the central vortices of circulation $+1$ and $+2$ in components $j = 0$ and -1 , respectively. However, for a spin-1 SO-coupled spinor BEC of type $(-1, 0, +1)$, rotating with the angular momentum vector anti-parallel to the vorticity direction, for small angular frequency of rotation, the state $(-1, 0, +1)$ transforms into the state $(-2, -1, 0)$. With the increase of angular frequency of rotation, an anti-vortex lattice with hexagonal symmetry can again

be generated maintaining these central anti-vortices of circulation -2 and -1 in the respective components.

In the case of a rotating SO-coupled spin-1 spinor condensate, we find that there are many different vortex-lattice states with different symmetry properties lying close to each other. Hence it is often difficult to find the vortex-lattice state with minimum energy by imaginary-time propagation and it is possible that, in some cases, the imaginary-time approach converges to a nearby excited vortex-lattice state, instead of the lowest-energy state for certain initial states. To circumvent this problem, we repeated the calculation with different initial states, so as to be sure that the converged vortex-lattice state is indeed the lowest-energy state. The use of an analytic initial function modulated by a random phase at different space points also increases the possibility of the convergence to the minimum-energy state [10]. Unlike in a rotating scalar BEC, where the vortex lattice in the lowest-energy state always has a hexagonal symmetry, in the case of a rotating SO-coupled spin-1 spinor BEC, vortex- and anti-vortex-lattice states with an approximate square symmetry can also appear, in addition to those with the usual hexagonal symmetry. For hexagonal symmetry, vortices are arranged in concentric orbits containing a maximum of 6, 12, 18 ... vortices; for square symmetry these numbers are 8, 12, 16 ... Often, for the same angular frequency of rotation, it is possible to obtain both types of vortex-lattice states with all orbits containing the maximum number of vortices. When this happens, the vortex- and anti-vortex-lattice states for both ferromagnetic and anti-ferromagnetic SO-coupled spin-1 BECs with square symmetry are found to have the smaller numerical energy, although we could not establish this fact theoretically. The general scenario of vortex-lattice states remain unchanged for different numerical values of the non-linearity parameters c_0 and c_2 .

B. Ferromagnetic condensate

We study the formation of vortex-lattice states with hexagonal symmetry in a rotating Rashba SO-coupled quasi-2D ^{87}Rb ferromagnetic spin-1 BEC with SO-coupling strength $\gamma = 0.5$, and non-linearities $c_0 = 1327$ and $c_2 = -6.15$ for different angular frequency Ω through a plot of contour density $n_j(\boldsymbol{\rho}) = |\psi_j(\boldsymbol{\rho})|^2$ of different components. In figures 1(a)-(c) we plot the densities of components $j = +1, 0, -1$ of the non-rotating lowest-energy circularly-symmetric state of type $(0, +1, +2)$. We checked the vorticity and circulation of the components analyzing the phase plot of the wave function displayed in figures 2(a)-(c). The phase drop upon a clockwise rotation of 2π in figure 2(b) (c) is 2π (4π) indicating a circulation of $+1$ ($+2$). The $j = -1$ component with circulation $+2$ has a larger vortex core than the $j = 0$ component with circulation $+1$. In figures 1(d)-(f) we display the vortex lattice with hexagonal symmetry for increasing angular frequencies $\Omega = 0.4, 0.65$, and 0.835 . The

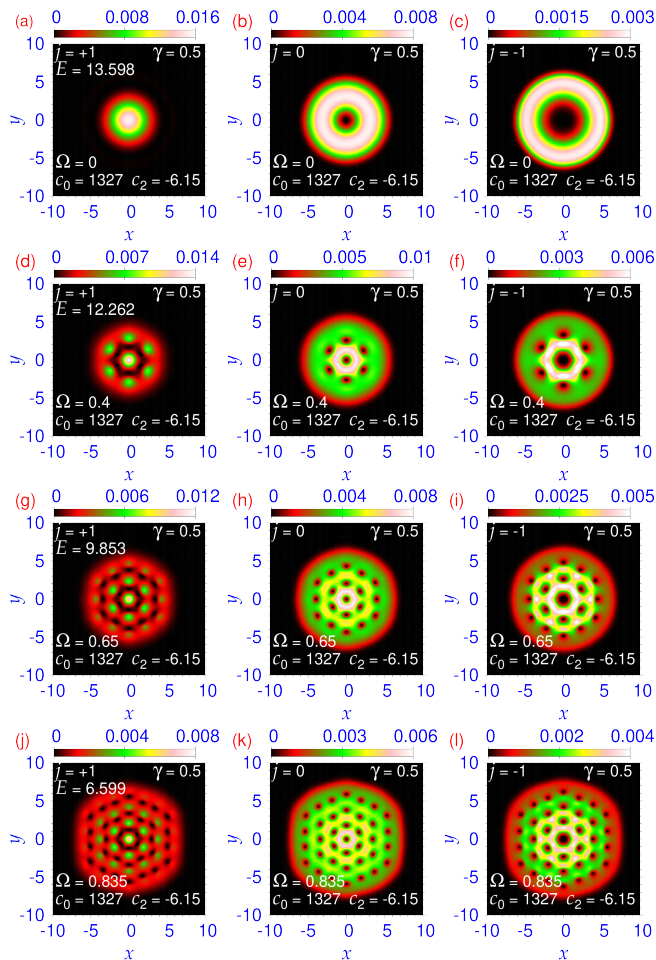


FIG. 1: (Color online) Contour plot of component densities $n_j(\boldsymbol{\rho}) \equiv |\psi_j(\boldsymbol{\rho})|^2$ of vortex-lattice states with hexagonal symmetry of a rotating Rashba SO-coupled ferromagnetic spin-1 quasi-2D spinor BEC for angular frequencies $\Omega = 0, 0.4, 0.65$, and 0.835 in plots (a)-(c), (d)-(f), (g)-(i), and (j)-(l), respectively. The angular momentum of rotation is parallel to the vorticity direction of the non-rotating state in (a)-(c). The non-linearity parameters $c_0 = 1327, c_2 = -6.15$, and SO-coupling strength $\gamma = 0.5$. In all density plots of this paper, energy values, viz. (8), are displayed in the density of the $j = +1$ component. All results reported in this paper are in dimensionless units, as outlined in Section II.

vortex structure of the BEC with $\Omega = 0.4$ can be found from the phase plot of the corresponding wave function in figures 2(d)-(f) for components $j = +1, 0, -1$. The direction of generated angular momentum upon rotation is parallel to the intrinsic vorticity of the non-rotating state (z direction). For all angular frequencies, a clean vortex lattice is generated as in the case of a scalar BEC. The only difference from a scalar BEC is that the central spot is vortex free for component $j = +1$ and hosts a vortex of circulation $+2$ in component $j = -1$. In the component $j = 0$, the central spot has a vortex of circulation $+1$ as in a scalar BEC. A vortex of circulation $+2$ (greater than unity) in a scalar BEC should break into two of unit

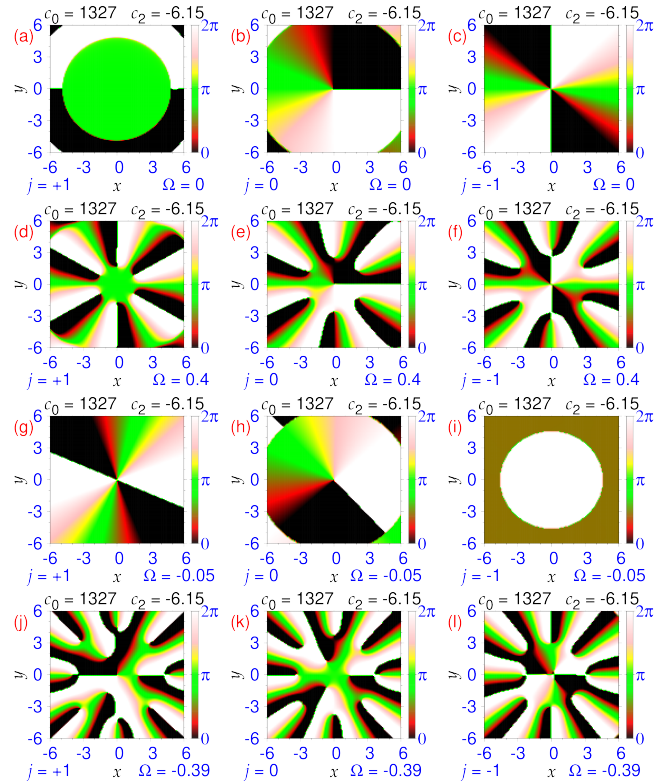


FIG. 2: (Color online) (a)-(c) Contour plot of the phase $\delta(\boldsymbol{\rho})$ of the wave function of the non-rotating Rashba SO-coupled ferromagnetic spin-1 quasi-2D spinor BEC of figures 1(a)-(c). (d)-(f) The same of the rotating ferromagnetic spinor BEC, with angular frequency $\Omega = 0.4$, of figures 1(d)-(f). (g)-(i) The same of the rotating ferromagnetic spinor BEC, with angular frequency $\Omega = -0.05$, of figures 4(a)-(c). (j)-(l) The same of the rotating ferromagnetic spinor BEC, with angular frequency $\Omega = -0.39$, of figures 5(a)-(c).

circulation from an energetic consideration [7]. However, in this SO-coupled spin-1 spinor BEC, the vortex of circulation $+2$ at the center of component $j = -1$ is found to be energetically stable.

For the same sets of parameters as in figure 1, the vortex-lattice states with an approximate square symmetry are shown in figures 3(a)-(i) for angular frequencies $\Omega = 0.4, 0.65$, and 0.835 , where vortices are arranged in approximate concentric square orbits with 8, 12, and 16 vortices. The central spot in components $j = 0$ and -1 has a vortex of circulation $+1$ and $+2$, respectively, whereas the same in component $j = +1$ is vortex free. In table I we display the respective energies of the vortex-lattice states of figures 1 and 3 and find that the states of figure 3 have smaller energies as compared to the respective states in figure 1.

Next we consider the formation of vortex lattice in a quasi-2D Rashba SO-coupled ferromagnetic spin-1 spinor BEC upon rotation with angular momentum opposite to the intrinsic vorticity of the non-rotating BEC, denoted by negative values of angular frequency Ω in (4)

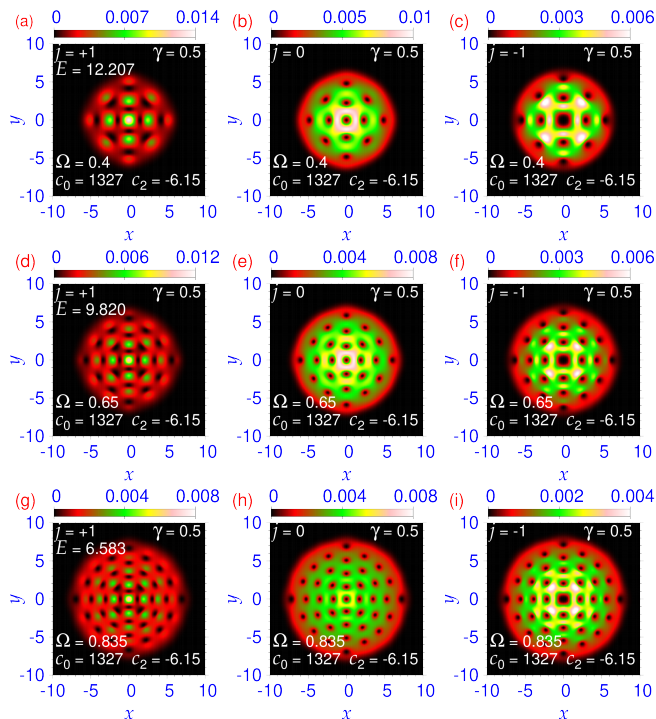


FIG. 3: (Color online) The same as in figure 1 with approximate square symmetry for angular frequencies $\Omega = 0.4, 0.65,$ and 0.835 in (a)-(c), (d)-(f), and (g)-(i), respectively. The parameters of the ferromagnetic BEC are the same as in figure 1.

and (5). The contour plots of generated vortex lattices with hexagonal symmetry for angular frequencies $\Omega = -0.05, -0.39, -0.62$ and -0.82 are shown in figures 4(a)-(c), (d)-(f), (g)-(i), (j)-(l), respectively. In all plots of figure 4 the circulation of rotation has opposite sign

TABLE I: (Color online) Energy of the different vortex-lattice and anti-vortex-lattice states of hexagonal and approximate square symmetry for a ferromagnetic and anti-ferromagnetic (polar) BEC and the corresponding minimum energy state. In all cases the lattice has all concentric orbits with the maximum number of vortices.

Ω	E (hexagonal)	E (square)	minimum energy state
+0.4	12.262	12.207	square
+0.65	9.853	9.820	square
ferro +0.835	6.599	6.583	square
-0.39	12.315	12.264	square
-0.62	10.203	10.192	square
-0.82	6.921	6.915	square
+0.55	6.751	6.621	square
+0.795	4.539	4.512	square
polar -0.55	6.751	6.715	square
-0.79	4.598	4.575	square

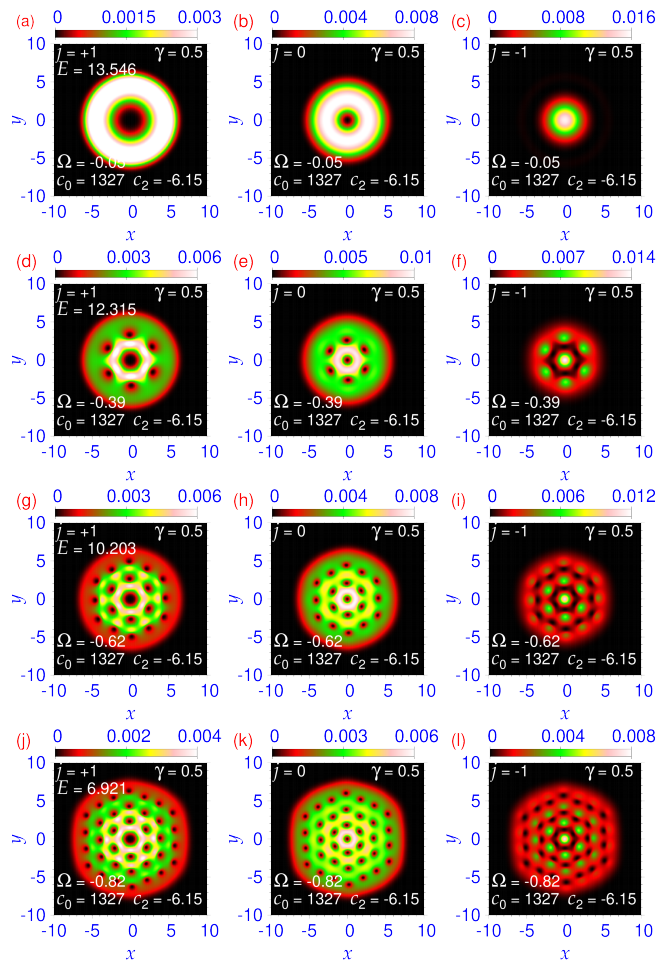


FIG. 4: (Color online) The same as in figure 1 for angular frequencies $\Omega = -0.05, -0.39, -0.62,$ and -0.82 in plots (a)-(c), (d)-(f), (g)-(i), and (j)-(l), respectively. The angular momentum of rotation is anti-parallel to the vorticity direction of the non-rotating state in figures 1(a)-(c). The parameters of the ferromagnetic BEC are the same as in figure 1.

compared to the same in figures 1 and 3. Hence these vortices are anti-vortices. Upon rotation of the state of type $(0, +1, +2)$ of figures 1(a)-(c) with angular frequency $\Omega = -0.05$, with opposite vorticity, a state of type $(-2, -1, 0)$ is generated as shown in figures 4(a)-(c). The opposite vorticity of the vortices in figures 4(a)-(c), as compared to those in figures 1(a)-(c), was confirmed from a plot of the corresponding phase in figures 2(g)-(i). The phase drop upon a clockwise rotation of 2π in figures 2(g) (h) is -4π (-2π) indicating an anti-vortex of circulation -2 (-1), viz. compare with vortices in figures 2(b)-(c). As angular frequency $|\Omega|$ is increased, an anti-vortex lattice with hexagonal symmetry is generated in the three components maintaining the anti-vortices $(-2, -1, 0)$ at the center, viz. figures 4(d)-(f), 4(g)-(i), and 4(j)-(l), for $\Omega = -0.39, -0.62,$ and -0.82 , respectively.

Apart from the anti-vortex lattice with hexagonal symmetry of figure 4, one can also have the same with approx-

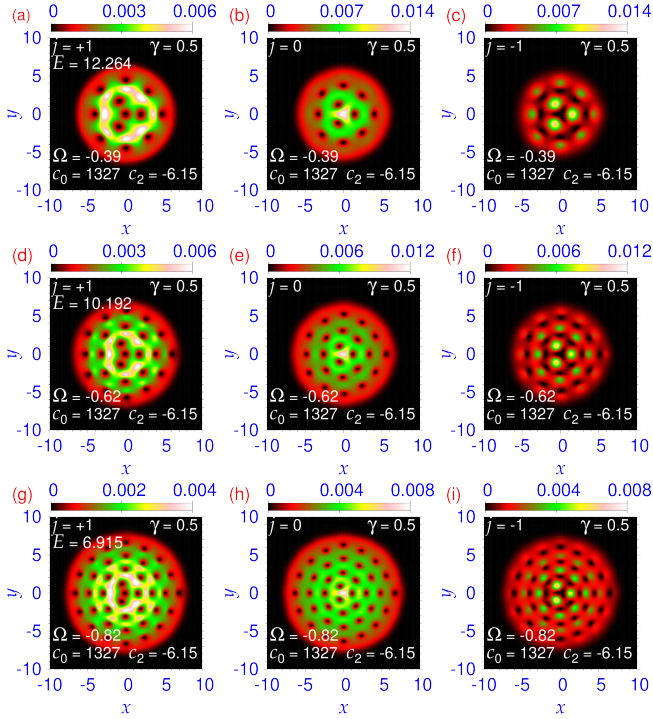


FIG. 5: (Color online) The same as in figure 4 with approximate square symmetry for angular frequencies $\Omega = -0.39, -0.62$, and -0.82 in (a)-(c), (d)-(f), and (g)-(i), respectively. The angular momentum of rotation is anti-parallel to the vorticity direction of the non-rotating state in figures 1(a)-(c). The parameters of the ferromagnetic BEC are the same as in figure 4.

imate square symmetry for the same angular frequencies $\Omega = -0.39, -0.62$ and -0.82 as shown in figures 5(a)-(c), (d)-(f) and (g)-(i), respectively. The central part in figure 5 has 4 and 3 anti-vortices of unit circulation in components $j = +1$ and 0, and an anti-vortex of circulation -2 in component $j = -1$. The net circulation of the anti-vortex at the center of component $j = -1$ was obtained from a consideration of the phase plot of the wave function for $\Omega = -0.39$ as displayed in figures 2(j)-(l). The phase drop upon a clockwise rotation of 2π in figure 2(l) is -4π indicating a circulation of -2 in component $j = -1$. The other anti-vortices of unit circulation in figures 5(a)-(c) can be identified in the phase plots in figures 2(j)-(l). This central part is a superposition of the non-rotating state $(0, +1, +2)$ and the state $(-4, -4, -4)$ generated by rotation. The energies of the anti-vortex-lattice states with hexagonal and square symmetries of figure 4 and 5 are shown in table I for angular frequencies $\Omega = -0.39, -0.62$ and -0.82 .

C. Anti-ferromagnetic condensate

The vortex-lattice formation with hexagonal symmetry in an anti-ferromagnetic rotating Rashba SO-coupled

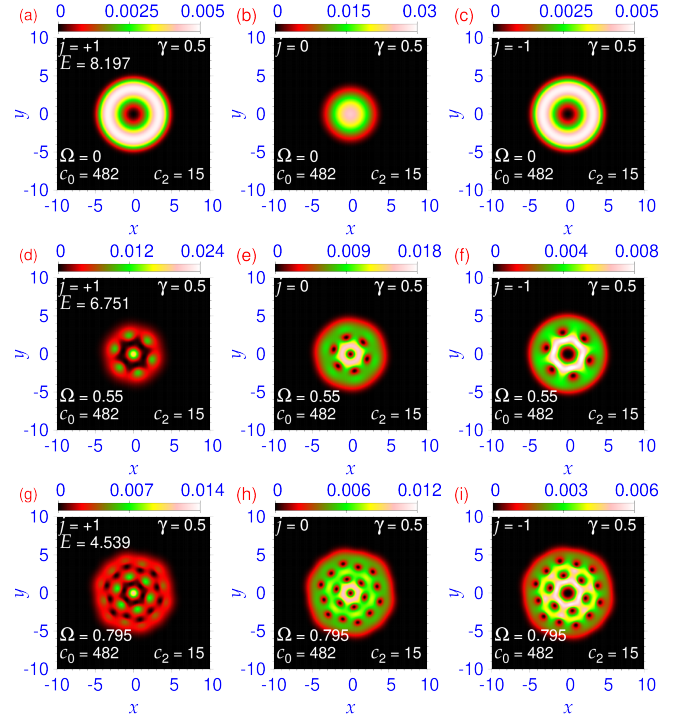


FIG. 6: (Color online) Contour plot of component densities $n_j(\boldsymbol{\rho}) \equiv |\psi_j(\boldsymbol{\rho})|^2$ of vortex-lattice states of a rotating Rashba SO-coupled anti-ferromagnetic spin-1 quasi-2D spinor BEC with hexagonal symmetry for angular frequencies $\Omega = 0, 0.55$, and 0.795 , in plots (a)-(c), (d)-(f), and (g)-(i), respectively. The angular momentum of rotation is parallel to the vorticity direction of the vortex in component $j = -1$ in (c). The non-linearity parameters $c_0 = 482, c_2 = 15$, and SO-coupling strength $\gamma = 0.5$.

quasi-2D ^{23}Na spin-1 BEC with SO-coupling strength $\gamma = 0.5$, and non-linearities $c_0 = 482$ and $c_2 = 15$ is demonstrated in figure 6. The non-rotating state ($\Omega = 0$), in this case, is of the $(-1, 0, +1)$ type as shown in figures 6(a)-(c) through a contour plot of densities. The vortex and anti-vortex nature of the two states is confirmed from the corresponding phase plot of the wave function (not shown here). Upon rotation, the $(-1, 0, +1)$ -type state, with the appearance of a vortex of circulation $+1$ in all components, transforms into a state of the $(0, +1, +2)$ type. These vortices of circulation $+1$ and $+2$ at the center of components $j = 0$ and -1 are maintained in the vortex lattice with hexagonal symmetry of a rapidly rotating anti-ferromagnetic quasi-2D spin-1 spinor BEC as in the case of a rapidly rotating ferromagnetic spin-1 spinor BEC considered in figure 1. We display the formation of vortex lattice with hexagonal symmetry in the anti-ferromagnetic spinor BEC for angular frequencies $\Omega = 0.55$, and 0.795 in figures 6(d)-(f), (g)-(i), respectively. We checked the vorticity and circulation of the components analyzing the phase plot of the wave function of the BEC displayed in figures 6(d)-(f), viz. Figs. 7(a)-(c). The phase drop upon a clockwise

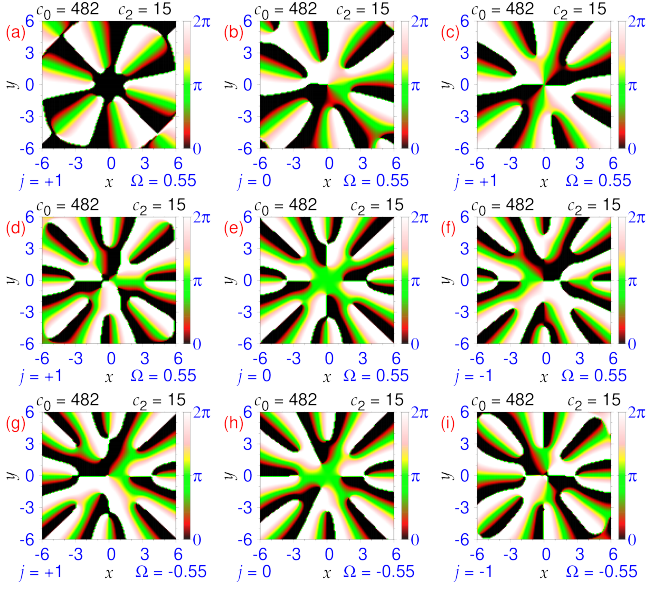


FIG. 7: (Color online) (a)-(c) Contour plot of the phase $\delta(\rho)$ of the wave function of the rotating anti-ferromagnetic spinor BEC, with angular frequency $\Omega = 0.55$, of figures 6(d)-(f). (d)-(f) The same of the rotating anti-ferromagnetic spinor BEC, with angular frequency $\Omega = 0.55$, of figures 8(a)-(c). (g)-(i) The same of the rotating anti-ferromagnetic spinor BEC, with angular frequency $\Omega = -0.55$, of figures 10(a)-(c).

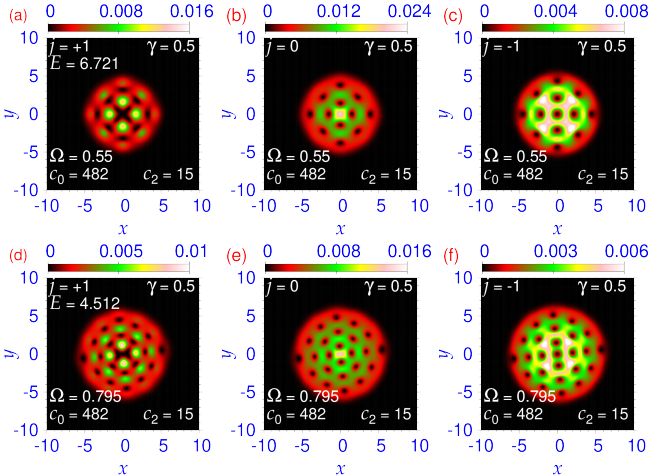


FIG. 8: (Color online) The same as in figure 6 with approximate square symmetry with angular frequencies $\Omega = 0.55$ and 0.795 in (a)-(c) and (d)-(f), respectively. The parameters of the anti-ferromagnetic BEC are the same as in figure 6.

rotation of 2π in figure 7(b) (c) is 2π (4π) indicating circulation $+1$ ($+2$) at the center. The $j = -1$ component with circulation $+2$ has a larger vortex core than the $j = 0$ component with circulation $+1$. The hexagonal vortex lattices in figure 6 for an anti-ferromagnetic spin-1 spinor BEC are quite similar to the vortex lattices in figure 1 for a ferromagnetic spinor BEC.

Next we consider the formation of vortex lattice with

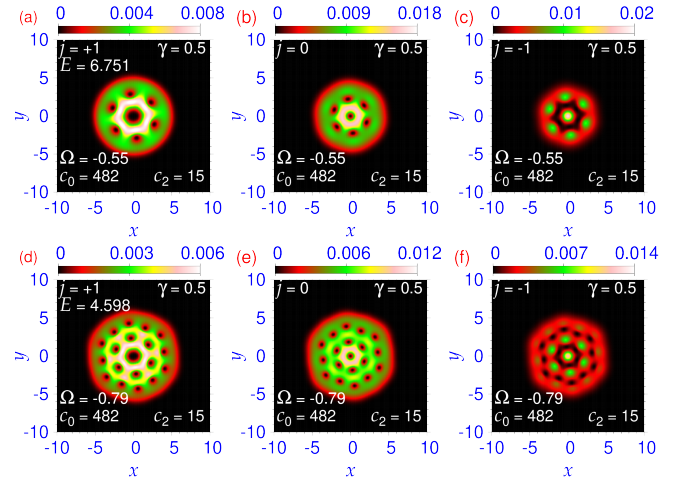


FIG. 9: (Color online) The same as in figure 6 for angular frequencies $\Omega = -0.55$, and -0.79 , in (a)-(c), and (d)-(f), respectively. The angular momentum of rotation is anti-parallel to the vorticity direction of the vortex in component $j = -1$ in figure 6 (c). The parameters of the anti-ferromagnetic BEC are the same as in figure 6.

approximate square symmetry in a Rashba SO-coupled anti-ferromagnetic quasi-2D spinor BEC upon rotation. The resultant vortex lattices, in this case, for angular frequencies $\Omega = 0.55$ and 0.795 are displayed in figures 8(a)-(c) and (d)-(f), respectively. The central region of the vortex lattice, in this case, is different from that in figure 6. The central region is formed by a superposition of the $(-1, 0, +1)$ -type state of the non-rotating BEC, viz. figures 6(a)-(c), with a $(+4, +4, +4)$ -type state formed by rotation, thus resulting in a state with vortex of circulation $+3$ ($+4, +5$) in component $j = +1$ ($j = 0, j = -1$). The vortex of circulation $+4$ ($+5$) in component $j = 0$ ($j = -1$) breaks into 4 (5) vortices of unit circulation, whereas the $j = +1$ component contains a complex vortex structure of circulation $+3$, as can be seen from a phase plot of the wave function of the condensate displayed in figures 8 (a)-(c), viz. figures 7(d)-(f). In the outer region we have vortices arranged in concentric square orbits with 8 and 12 vortices, viz. figures 8(a)-(c) and (d)-(f). Hence, although the vortex lattices with hexagonal symmetry in figures 1 and 6 are quite similar, those with approximate square symmetry in figures 3 and 8 for ferromagnetic and anti-ferromagnetic spinor BECs are different in the central region maintaining similarity in the outer region.

Let us next consider the formation of anti-vortex lattice with hexagonal symmetry in a rotating Rashba SO-coupled anti-ferromagnetic spinor BEC with the angular momentum of rotation opposite to the vorticity direction of the vortex in component $j = -1$ of figure 6(c). The non-rotating state in figures 6(a)-(c) is of the $(-1, 0, +1)$ type. For small angular frequency of rotation, an anti-vortex is generated in all three components in the form of a $(-1, -1, -1)$ -type state, which when superposed on the

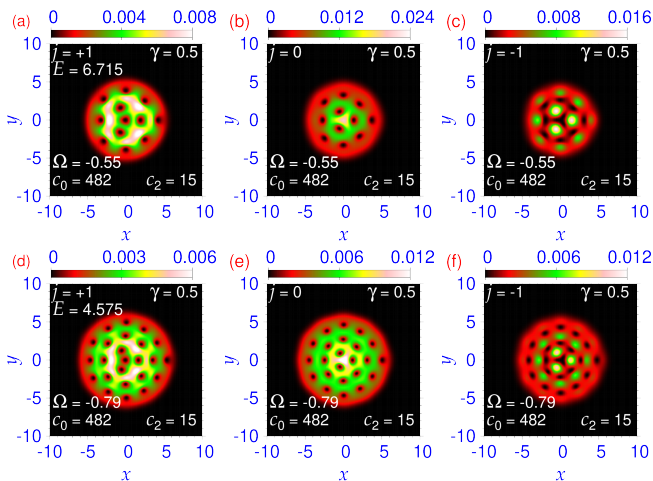


FIG. 10: (Color online) The same as in figure 6 with approximate square symmetry with angular frequencies $\Omega = -0.55$, and -0.79 , in (a)-(c), and (d)-(f) respectively. The angular momentum of rotation is anti-parallel to the vorticity direction of the vortex in component $j = -1$ in figure 6 (c). The parameters of the anti-ferromagnetic BEC are the same as in figure 6.

$(-1, 0, +1)$ -type state leads to a $(-2, -1, 0)$ -type state at the center. The generated anti-vortex lattice in this case maintains this scenario in the central region, e.g., one (two) anti-vortex of circulation -1 in component $j = 0$ ($j = +1$) and none in component $j = -1$, around which the hexagonal vortex lattice is formed. This is illustrated by a plot of contour density of components $j = +1, 0, -1$ for angular frequencies $\Omega = -0.55$, and -0.79 in figures 9(a)-(c), and (d)-(f), respectively. The generated anti-vortex lattice states in figure 9 for the anti-ferromagnetic phase are identical to those figure 4 for the ferromagnetic phase.

Finally, we consider the formation of anti-vortex lattice with square symmetry in a rotating SO-coupled anti-ferromagnetic spinor BEC with the angular momentum of rotation opposite to the vorticity direction of the vortex in component $j = -1$, viz. figure 6(c). In this case, the generated anti-vortex lattice displayed in figure 10 for $\Omega = -0.55$ and -0.79 is quite similar to the anti-vortex lattice in the case of a ferromagnetic spinor BEC presented in figure 5. The vortices for $\Omega = -0.55$ can be identified from a phase plot of the wave function in figures 7(g)-(i). The anti-vortex lattice with square symmetry for $\Omega = -0.55$, and -0.79 is presented in figures 10(a)-(c), and (d)-(f) respectively. In table I we also display the energies of anti-vortex-lattice states of hexagonal and square symmetries of figures 9 and 10. The energies of the hexagonal anti-vortex-lattice states are larger than the corresponding states with square symmetry in all cases.

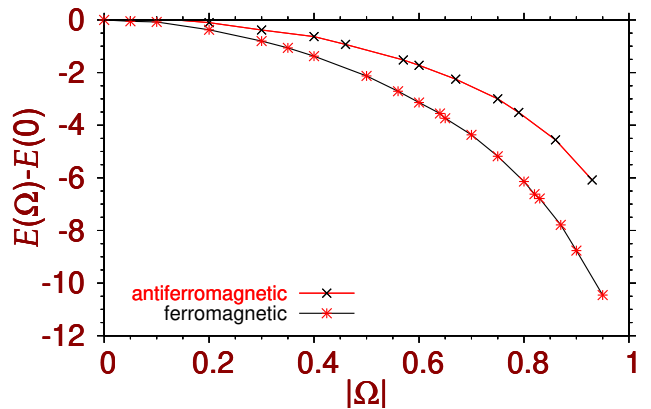


FIG. 11: (Color online) The rotational energy in the rotating frame $[E(\Omega) - E(0)]$ versus angular frequency of rotation for the ferromagnetic and anti-ferromagnetic BEC. The points are numerically calculated whereas the lines are to guide the eye.

IV. DISCUSSION

We now compare the present results of vortex-lattice formation in a Rashba SO-coupled spin-1 BEC with previous results [24–26] for vortex-lattice formation in a Rashba SO-coupled pseudo spin-1/2 BEC. A Rashba SO-coupled pseudo spin-1/2 BEC supports a half-quantum vortex state with an unit vortex in one component and zero vortex in the other, which is a $(+1, 0)$ -type state with intrinsic vorticity. This state should be compared with $(-1, 0, +1)$ - and $(0, +1, +2)$ -type states in the present Rashba SO-coupled spin-1 BEC. The vortex lattice for the pseudo spin-1/2 BEC has a vortex of unit circulation at the center of one component, whereas the center of the other component has no vortex in analogy with vortices of circulation 0, $+1$, and $+2$ at the centers of the three components, viz. figures 1(d)-(f), in the ferromagnetic case. The presence of the $(+1, 0)$ -type state with intrinsic vorticity in a pseudo spin-1/2 BEC breaks the symmetry between rotation with vorticity along the z and $-z$ axes and thus might generate different vortex-lattice and anti-vortex-lattice states in a rotating SO-coupled quasi-2D pseudo spin-1/2 BEC for these two types of rotation. However, the previous studies [24, 26] did not explore this possibility. The detailed numerical study [25] for vortex-lattice formation in the pseudo spin-1/2 case confirmed the formation of lattice with hexagonal symmetry only. In this study on the spin-1 BEC, in addition, we also demonstrate the formation of lattice with square symmetry.

The rotational energy of a scalar BEC $[E(\Omega) - E(0)]$ in the rotating frame is the energy of rigid-body rotation $\sim -I\Omega^2/2$ where I is the moment of inertia of the condensate. This energy is proportional to the square of the angular frequency [7], where $E(\Omega)$ is given by (8). In the case of spin-1 spinor ferromagnetic and anti-ferromagnetic BECs, a similar relation also

holds. We illustrate in figure 11 the rotational energy of the vortex- and anti-vortex-lattice states of both ferromagnetic and anti-ferromagnetic BECs with square and hexagonal symmetry as a function of angular frequency Ω , where we plot the energy of the minimum-energy state versus $|\Omega|$. The energies of ferromagnetic and anti-ferromagnetic BECs lie on two distinct lines showing similar qualitative behavior. The energy decreases with increasing angular frequency of rotation as the contribution of the rotational energy $-\Omega L_z$ in the expression for energy (8) is negative for large $|\Omega|$. For small Ω , in the perturbative limit, this contribution is linearly proportional to Ω . Hence as $\Omega \rightarrow 0$ ($\Omega \lesssim 0.1$), the rotational energy for positive (negative) values of Ω is positive (negative). For $\Omega \gtrsim 0.1$ rotational energies for both positive and negative Ω are negative. For $\Omega \gtrsim 0.2$ these two energies are practically equal and negative. The difference between the energies for $\pm\Omega$ is small and for clarity of the plot, this detail is not displayed in figure 11 and an average of the two energies are exhibited for small $|\Omega|$. But as $|\Omega|$ increases, the rotational energy behaves as $\sim -\Omega^2$ [7].

V. SUMMARY

We studied the formation of vortex lattice in a quasi-2D Rashba SO-coupled spin-1 spinor BEC in the $x - y$ plane, under rapid rotation, using the mean-field GP equation in the rotating frame, where the generated vortex-lattice state is a stationary state. In the case of a scalar BEC, the generated vortex lattice for rotation with vorticity along z and $-z$ axes are the same. The lowest-energy circularly-symmetric state of a non-rotating ferromagnetic Rashba SO-coupled spin-1 spinor BEC is of the $(0, +1, +2)$ type, whereas the same for an anti-ferromagnetic BEC is of the type $(-1, 0, +1)$. The intrinsic vorticity of these two states make the rotation with vorticity along z and $-z$ axes conceptually different for an SO-coupled spin-1 spinor BEC. Consequently, different from a scalar BEC, the generated vortex-lattice structure for a quasi-2D Rashba SO-coupled spin-1 spinor BEC for rotation with vorticity along z and $-z$ axes are different. For rotation with vorticity along z direction, a vortex lattice is formed and for rotation with vortic-

ity along $-z$ direction an anti-vortex lattice is formed. Two types of vortex and anti-vortex lattices were found to be formed predominantly: a hexagonal lattice and an approximate square lattice. For rotation with vorticity along z direction, the hexagonal lattice has vortices arranged in closed concentric orbits which accommodate the following maximum number of vortices: 6, 12, 18 etc., whereas the square lattice has vortices arranged in closed concentric orbits with the maximum numbers 8, 12, 16 etc. We illustrated, for different angular frequencies, the formation of vortex lattices with closed concentric orbits of vortices while all orbits accommodate the allowed maximum number of vortices. The central region in both cases is occupied by a complex structure of vortices, often accommodating vortices of circulation (angular momentum) greater than unity. In case of a scalar BEC, all vortices in a vortex lattice are of unit circulation. For rotation with vorticity along $-z$ axis, similar lattice structure emerges but with anti-vortices replacing vortices, although the central region of the lattice may have a different distribution of vortices from the case of rotation with vorticity along z axis. Such a lattice structure is termed an anti-vortex lattice as opposed to a vortex lattice. If, for a fixed angular frequency of rotation, both a square and a hexagonal vortex or anti-vortex lattice can be formed, with closed concentric orbits, the square vortex-lattice structure is found to possess the smaller energy as shown in table I. This strongly suggests the square lattice states to be the lowest-energy state. For larger values of γ (not considered in this paper), we could not find the hexagonal lattice states; only square lattice states were found. The rotational energy of the generated vortex or anti-vortex lattice for both ferromagnetic and anti-ferromagnetic BECs is found to be proportional to the square of angular frequency Ω as displayed in figure 11, consistent with a theoretical suggestion by Fetter for a scalar BEC [7].

Acknowledgments

S.K.A. acknowledges support by the CNPq (Brazil) grant 301324/2019-0, and by the ICTP-SAIFR FAPESP (Brazil) grant 2016/01343-7.

References

-
- [1] Anderson M H, Ensher J R, Matthews M R, Wieman C E and Cornell E A 1995 *Science* **269** 198
 - [2] Madison K W, Chevy F, Wohlleben W and Dalibard J 2000 *Phys. Rev. Lett.* **84** 806
 - [3] Abo-Shaer J R, Raman C and Ketterle W 2002 *Phys. Rev. Lett.* **88** 070409
 - [4] Onsager L 1949 *Nuovo Cimento*. **6** 249 supp 2
 - [5] Feynman R P 1955 *Prog. Low Temp. Phys.* **1** 17
 - [6] Abrikosov A A 1957 *Zh. Eksp. Teor. Fiz.* **32** 1442 [Eng. Transla. 1957 *Sov. Phys.-JETP* **5** 1174]
 - [7] Fetter A L 2009 *Rev. Mod. Phys.* **81** 647
 - [8] Vinen W F 1961 *Proc. R. Soc. Lond. A* **260** 218 (1961)
 - [9] Gordon M J V, Williams G A and Packard R E 1978 *J. Phys. (Paris)* **39** C6-172
 - [9] London F 1938 *Nature* **141** 643

- [10] Kumar R K, Lončar V, Muruganandam P, Adhikari S K and Balaž A 2019 *Comput. Phys. Commun.* **240** 74
- [11] Stenger J, Inouye S, Stamper-Kurn D M, Miesner H-J, Chikkatur A P and Ketterle W 1998 *Nature* **396** 345
- [12] J. Dalibard, F. Gerbier, G. Juzeliūnas, P. Öhberg, *Rev. Mod. Phys.* **83**, 1523 (2011).
- [13] Rashba E I 1960 *Fiz. Tverd. Tela* **2** 1224 [English Transla.: 1960 *Sov. Phys. Solid State* **2** 1109]
- [14] Dresselhaus G 1955 *Phys. Rev.* **100** 580
- [15] Lin Y-J, Jiménez-García K and Spielman I B 2011 *Nature* **471** 83
- [16] Li J, Huang W, Shteynas B, Burchesky S, Top F C, Su E, Lee J, Jamison A O and Ketterle W 2016 *Phys. Rev. Lett.* **117** 185301
- [17] Campbell D, Price R, Putra A, Valdés-Curiel A, Trypogeorgos D and Spielman I B 2016 *Nature Commun.* **7** 10897
- [18] Kawaguchi Y and Ueda M 2012 *Phys. Rep.* **520** 253
- [19] Mizushima T, Machida K and Kita T 2002 *Phys. Rev. A* **66** 053610
- [20] Mizushima T, Machida K and Kita T 2002 *Phys. Rev. Lett.* **89** 030401
- [21] Stamper-Kurn D M and Ueda M 2013 *Rev. Mod. Phys.* **85** 1191
- Ueda M 2014 *Rep. Prog. Phys.* **77** 122401
- [22] Mermin N D and Ho T-L 1976 *Phys. Rev. Lett.* **36** 594
- [23] Anderson P W and Toulouse G 1977 *Phys. Rev. Lett.* **38** 508
- [24] Xu X-Q and Han J H 2011 *Phys. Rev. Lett.* **107** 200401
- [25] Zhou X-F, Zhou J and Wu C 2011 *Phys. Rev. A* **84** 063624
- [26] Fetter A L 2014 *Phys. Rev. A* **89** 023629
- [27] Radić J, Natu S S and Galitski V 2014 *Phys. Rev. Lett.* **113** 185302
- Hickey C and Paramekanti A 2014 *Phys. Rev. Lett.* **113** 265302
- [28] Su S-W, Gou S-C, Sun Q, Wen L, Liu W-M, Ji A-C, Ruseckas J and Juzeliūnas G 2016 *Phys. Rev. A* **93** 053630
- [29] Li Y, Martone G I, Pitaevskii L P and Stringari S 2013 *Phys. Rev. Lett.* **110** 235302
- Martone G I, Pepe F V, Facchi P, Pascazio S and Stringari S 2016 *Phys. Rev. Lett.* **117** 125301
- [30] Li J-R, Lee J, Huang W, Burchesky S, Shteynas B, Top F Ç, Jamison A O and Ketterle W 2017 *Nature* **543** 91
- [31] Jiang L, Liu X-J, and Pu H 2011 *Phys. Rev. A* **84** 063618
- Vyasanakere J P and Shenoy V B 2012 *New J. Phys.* **14** 043041
- [32] König M, Wiedmann S, Brüne C, Roth A, Buhmann H, Molenkamp L W, Qi X-L and Zhang S-C 2007 *Science* **318** 766
- [33] Žutić I, Fabian J and Das Sarma S 2004 *Rev. Mod. Phys.* **76** 323
- [34] Chen X, Rabinovic M, Anderson B M and Santos L 2014 *Phys. Rev. A* **90** 043632
- Han W, Juzeliūnas G, Zhang W and Liu W-M 2015 *Phys. Rev. A* **91** 013607
- Su S-W, Gou S-C, Liu I-K, Spielman I B, Santos L, Acus A, Mekys A, Ruseckas J and Juzeliūnas G 2015 *New J. Phys.* **17** 033045
- [35] Sun K, Qu C, Xu Y, Zhang Y and Zhang C 2016 *Phys. Rev. A* **93** 023615
- Yu Z-Q 2016 *Phys. Rev. A* **93** 033648
- [36] Radić J, Sedrakyan T A, Spielman I B and Galitski V 2011 *Phys. Rev. A* **84** 063604
- [37] Ravisankar R, Vudragović D, Muruganandam P, Balaž A and Adhikari S K 2020 *Comput. Phys. Commun.* in press, doi.org/10.1016/j.cpc.2020.107657; arXiv:2009.13507.
- [38] Zhai H 2012 *Int. J. of Mod. Phys. B* **26** 1230001
- [39] Landau L D and Lifshitz E M 1960 *Mechanics* (Pergamon Press, Oxford), Section 39.
- [40] Salasnich L, Parola A and Reatto L 2002 *Phys. Rev. A* **65** 043614
- [41] Yukalov V I (2018) *Laser Phys.* **28** 053001
- [42] Gautam S and Adhikari S K 2015 *Phys. Rev. A* **92** 023616
- [43] Muruganandam P and Adhikari S K 2009 *Comput. Phys. Commun.* **180** 1888
- [44] Vudragović D, Vidanović I, Balaž A, Muruganandam P and Adhikari S K 2012 *Comput. Phys. Commun.* **183** 2021
- [45] Young-S. L E, Muruganandam P, Adhikari S K, Lončar V, Vudragović D, Balaž A 2017 *Comput. Phys. Commun.* **220** 503
- [46] van Kempen E G M, Kokkelmans S J J M F, Heinzen D J and Verhaar B J 2002 *Phys. Rev. Lett.* **88** 093201
- [47] Lim F Y and Bao W 2008 *Phys. Rev. E* **78** 066704
- Bao W and Lim F Y 2008 *Siam J. Sci. Comput.* **30** 1925